10.21611/qirt.2023.28

QIRT Asia 2023

4th Asian Quantitative InfraRed Thermography Conference

Thermomics: Temporal Thermography Features

by Leonardo D. Buitrago [1], Xavier P.V. Maldague [2,*], and Bardia Yousefi [1,2,*]

1 University of Maryland, College Park, MD 20850, USA
2 Laval University, Quebec City, QC G1V 0A6, Canada
* Co-senior authors and correspondence: Xavier.Maldague@ulaval.ca; byousefi@umd.edu

Abstract

Dynamic thermography has firmly established itself as a diagnostic tool for breast cancer screening, often employed in conjunction with mammography and Clinical Breast Examination (CBE). Thermomics or temporal dynamic thermographic imaging biomarkers, have demonstrated their ability in the identification of vasodilation and angiogenesis within breast tissue, serving as biomarkers to highlight abnormalities and lesions. The development of new blood vessels or angiogenesis is also revealed with the aid of heterogeneous thermal patterns. This study focused on an overall look at the *thermomics* and they are for CBE-based breast cancer screening. We showed an application of dynamic thermal image embedding approaches and their help to find breast thermal heterogeneity with the optimal number of low-rank factorization methods. Using ideal biomarkers holds the potential of maintaining thermal heterogeneity, facilitating the early detection of breast cancer, and can function as a non-invasive aid for CBE.

1. Introduction

Thermal dynamics, specifically the temporal evolution of thermographic features, have emerged as a valuable tool in the early detection of breast cancer, a disease ranking as the second leading cause of mortality among women [1]. These thermal dynamics are proposed for deployment in clinical breast examination (CBE) and as a preliminary screening modality preceding mammography, furnishing critical insights into potential abnormalities in patients [2,3]. The fundamental principle underpinning thermographic imaging resides in the observed augmentation of vasodilation and angiogenesis, the formation of new blood vessels, in the breast region attributed to irregular lesions. These endocrine shifts, instigated by breast lesions, induce alterations in the thermal profile, indicative of heightened vascularization essential for supplying oxygen and nutrients to these lesions [3,4]. The utilization of an infrared camera facilitates the capture of these alterations, ultimately leading to the identification of abnormalities. Several studies have substantiated the pivotal role of thermography in discerning hypervascularity in non-palpable breast cancer cases [4]. This phenomenon holds the potential to serve as a biomarker for the early detection of breast cancer during CBE and before conventional mammography.

Nonetheless, the primary challenge in the utilization of infrared technology for breast cancer detection centers around the intricate task of capturing irregularities and translating raw infrared sequences into coherent thermal patterns. To surmount this challenge, there has been widespread adoption of low-rank matrix approximation methods, wherein the essential basis of the decomposed eigenvector matrix is carefully chosen to extract the dominant images that faithfully represent the entire thermal data stream. A diverse array of techniques, including principal component analysis (PCA or PCT) [5,6], non-negative matrix factorization (NMF) [7], fixed eigenvector analysis [8], incremental PCA [9], sparse factorization [10], t-distributed stochastic neighbour embedding (t-SNE) [11], candid covariance-free incremental principal component thermography (CCIPCT) [12], sparse PCA [13,14], semi-NMF [15-17], sparse NMF [18], convex NMF [19], deep NMF [20], and deep learning convex [21], have been harnessed in the domain of thermography to address these computational complexities.

Efficiently extracting the low-rank matrix representation characterized by maximum thermal pattern variance hinges on the selection of the most appropriate basis, a task that introduces an additional layer of complexity. To tackle this challenge, embedding techniques have been integrated into the analysis of low-rank approximation for dynamic thermography, as demonstrated in this study. The research advocates for the utilization of the most dominant basis in conjunction with embedding to extract thermomic features and subsequently train a classifier tailored for the early diagnosis of breast abnormalities. Notably, the proposed embedding functions offer superior representations of the underlying normal distribution compared to the previously employed low rank matrix factorization techniques. This advancement holds the potential to yield more precise representations of thermal patterns and, consequently, a more effective thermal diagnostic biomarker.

2. Method

2.1. Low-Rank Matrix approximation

Input data X is a stack of vectorized thermal images, a heat matrix. A low-rank representation model is shown as follows:

$$\mathrm{X} \approx \mathrm{BA} \tag{1}$$

where $\mathrm{X} \in \mathbb{R}^{\mathrm{MN}\times\tau}$, i.e., $\mathrm{X} = [\mathbf{x_1}, \mathbf{x_2}, \dots, \mathbf{x_\tau}]$ and can be shown by a linear combination of τ bases, $\mathrm{B} = \{\boldsymbol{\beta_1}, \boldsymbol{\beta_2}, \dots, \boldsymbol{\beta_\tau}\}, \mathrm{B} \in \mathbb{R}^{\mathrm{MN}\times\tau}$ and A, a coefficient matrix, $\mathrm{A} \in \mathbb{R}^{\tau\times\tau}$, $\mathrm{A} = \{\alpha_1, \alpha_2, \dots, \alpha_\tau\}$. $\mathbf{x}_1, \mathbf{x}_2, \dots, \mathbf{x}_\tau$ are vectorized thermal images and correspond

License: https://creativecommons.org/licenses/by-nd/4.0/deed.en

to τ frames. X is normalized stacked of many thermal tensors obtained from input thermal images. Bases and coefficients can be modified depending on which eigen decomposition or matrix factorization method is used.

2.2. Sparse Low-Rank Matrix approximation

Previous works have also shown different approaches to extracting thermomics. Sparse low-rank matrix approximation was previously used to extract them from different thermal images [18]. The factorization methods used were sparse PCT and semi-, convex- and sparse- NMF. PCT decomposes the input data X to $\mathrm{U}\sum\mathrm{V}^{\mathrm{T}}$ where U and $\sum$ represent eigenvector and eigenvalue matrices [18]. Sparse-PCT in contrast is defined as follows:

$$\sum_{\mathrm{i}=1}^{\Delta} ||\mathbf{x}_{\mathrm{i}} - \mathrm{AB}^{\mathrm{T}}||^2 + \lambda||\mathrm{B}||^2 \quad \mathrm{S.T.} \quad \mathrm{A}^{\mathrm{T}}\mathrm{A} = 1 \tag{2}$$

Where sparse-PCT optimizes the selection of bases with the addition of penalty terms in which increases the sparsity of three NMF methods as NMF assumes matrices X, B, and A are non-negative $(\mathrm{X} = \mathrm{BA})$[18]. Semi-NMF performs the matrix composition where A is still nonnegative, but B has no restriction represented by:

$$\mathbf{x} = \mathrm{BA}_{\mathrm{semiNMF}} \qquad \mathrm{S.T.} \qquad \mathrm{A} \leq 0, \mathrm{B} \geq 0 \tag{3}$$

Convex-NMF on the other hand imposes a constraint of the basis vectors lying within the column space of X. X in this case is defined as a linear combination of τ bases, $\mathrm{B} = [\boldsymbol{\beta}_1, \boldsymbol{\beta}_2, \dots, \boldsymbol{\beta}_\tau]$, and the coefficient A [18] represented by:

$$\mathrm{B} = \mathrm{XW} \qquad \mathrm{S.T.} \qquad \mathrm{A} \geq 0, \mathrm{W} \geq 0 \tag{4}$$

Sparse-NMF was proposed as a more robust way of thermal pattern extraction as it has minimal collinearity among bases compared to the semi- and convex- approaches as well as minimizing noise in the measurement of low-rank approximation. Sparse-NMF can be classified by the equation:

$$c_{sparse-NMF} = 1/2||\mathrm{X} - \mathrm{AB}||_{\mathrm{F}}^2 + \lambda||\mathrm{B}||_1 \tag{5}$$

Let $\|\mathrm{B}\|_p$ is the ℓ_p-norm of B given by $\ell_p = \sum_{\mathrm{d,m}} \left\|\mathrm{B}_{\mathrm{d,m}}\right\|_{\mathrm{p}}^{1/\mathrm{p}}$ similar to usual ℓ_1 penalty term to imitate the ℓ_0 behavior for calculating B for convex A [18,22]. The solution for all λ values is achieved through the Least Angle regression and selection algorithm. Results in the preservation of thermal heterogeneity using the NMF approaches provided accuracies of 74.1%, 75.9%, and 77.8%.

2.3. Embedding Thermography

The use of bases embedding has been proposed in previous studies [19,20,24], which involves combining multiple decomposed bases to reduce the dimensionality of thermal images. We previously applied low-rank representation methods to transform higher temporal dimensionality into lower temporal representations, which can be considered as bases computed using matrix factorization approaches [19]. We generate a set of low temporal dimensional represented bases ($\mathrm{B} = \{\boldsymbol{\beta}_1, \boldsymbol{\beta}_2, \dots, \boldsymbol{\beta}_\tau\}$, where $\mathrm{B} \in \mathbb{R}^{s \times \tau}, s = MN$)) and integrate their overall representation using two embedding membership functions [19,20,24]. This approach allows us to effectively reduce the dimensionality of presenting thermal images while preserving important information.

Definition 1. (From [19,20]) *The embedded low-dimensional representation,* $\boldsymbol{\Phi}$*, defines by aggregating membership calculated for p bases of* X, μ_p*, elementwise multiply by the basis itself,* $\boldsymbol{\beta}_i$*, and defined as:*

$$\boldsymbol{\Phi} = \sum_{i=1}^{p} \boldsymbol{\beta}_{\mathrm{i}} \odot \boldsymbol{\eta}_{\mathbf{i}} \tag{6}$$

where $\boldsymbol{\eta}_{\mathbf{i}}$ *is a membership on basis* $\boldsymbol{\beta}_{\mathrm{i}}$ *and defines by*:

$$\boldsymbol{\eta}_{\mathbf{i}} = \mathrm{e}^{\frac{\boldsymbol{\beta}_{\mathrm{i}} - \mu}{\sigma}}.$$

Let μ, σ mean (average) of a thermal image in the ROI basis and standard deviation of i^{th} −basis in the calculation. Letting μ, σ be the mean and standard deviation of the i^{th} thermal basis. We can also define Bell embedding as:

Definition 2. (From [24]) *The embedded low-rank matrix approximation,* $\dot{\boldsymbol{\Phi}}$*, defines by aggregating membership calculated for p bases of* X, μ_p*, elementwise multiply by the basis itself,* $\boldsymbol{\beta}_i$*, and defined as:*

$$\dot{\boldsymbol{\Phi}} = \sum_{\boldsymbol{i=1}}^{\boldsymbol{p}} \boldsymbol{\beta}_{\mathrm{i}} \odot \boldsymbol{\zeta}_{\boldsymbol{i}} \tag{7}$$

where $\boldsymbol{\zeta}_{\mathbf{i}}$ *is a membership on basis* $\boldsymbol{\beta}_{\mathrm{i}}$ *and defines by:*

$$\boldsymbol{\zeta}_{\mathbf{i}} = \frac{1}{1 + \left|\frac{\boldsymbol{\beta}_{\mathrm{i}} - \mu}{\sigma}\right|^{2\mathrm{b}}}.$$

With the variable b being an arbitrary coefficient in this case. $\boldsymbol{\zeta}_i$ is a generalized curve (Bell-shaped function) and a direct generalization of the *Cauchy* distribution. Thermomics extracted from the embedded bases subsequently lead to the automatic detection of breast cancerous leading abnormalities (CLA) which can be used for CBE and screening. The findings of this study validate the reliability of thermomics in the early detection of breast cancer and effectively highlight CLA in patients.

2.4. Deep-Learning Driven Thermomics

2.4.1. Hilbert Embedded Deep Low-Rank Matrix Factorization

As an improvement to the dimensionality reduction in the extraction of thermomics [20] using the deep low-rank NMF. We approach the overall decomposition process by sequentially decomposing the matrix $\mathrm{X} \approx \mathrm{B}_1\mathrm{A}_1$, and then further deconstructing B_1 in a recursive manner until all layers are fully decomposed. The utilization of Deep-SemiNMF results in the generation of a set of matrices $\mathrm{B}_1, \mathrm{B}_2, \mathrm{B}_3, \ldots, \mathrm{B}_\mathrm{m}$, where each B_i (for $i = \{1, \ldots, m\}$) corresponds to a distinct basis that captures specific patterns of heterogeneity within thermal images. In contrast, the application of SemiNMF in a shallow context yields a combined set of bases within a single matrix. Within the Deep-SemiNMF framework, we have the capacity to derive new features denoted as A^* by assuming that the weighted matrices (multi-layer bases) B_i remain fixed, and for all layers indexed by l, we have:

$$\mathrm{X} \approx \mathrm{B}_1\mathrm{A}_1 \approx \mathrm{B}_1\mathrm{B}_2\mathrm{A}_2 \approx \mathrm{B}_1\mathrm{B}_2\,\mathrm{B}_3 \ldots \mathrm{B}_\mathrm{m}\mathrm{A}^*$$

This dynamic formulation allows us to uncover and leverage intricate features across multiple layers to enhance the representational power of the model. We can learn new features A^*, by assuming that weighted matrices (multi-layer bases) $\forall i, \mathrm{B}_i$ are remain fixed and $\forall l, \mathrm{A}_l^*$ we have:

$$\underset{\mathrm{A}}{argmin}\left\|\mathbf{x}^* - \prod_{i=1}^{l} \mathrm{B}_i\mathrm{A}_l\right\| \qquad s.t.\ \mathrm{A}_l \geq 0. \tag{8}$$

where A_l, links to the l^{th} feature layer for the out-of-sample data point $\mathbf{x}^*$. Then the low-rank approximation was modified via the implementation of the Hilbert embedding method. This embedding method divided the thermomics set into several partitions. The Kernel value was then measured in each partition and the V-statistics are calculated among the features [20]. The dependency of the spanned thermomics' distribution was estimated using least absolute shrinkage and selection operator (lasso). The method for this is called HSIC Lasso, where HSIC defines as a given kernel matrix $\boldsymbol{K_q} \in \mathbb{R}^{\boldsymbol{\delta X \delta}}$ and offered an output criterion $\mathbb{C} \in \mathbb{R}^{\boldsymbol{\delta X \delta}}$[20]. With the use of the radial based function (RBF) Gaussian kernel, this method offered a scoring value to remove any redundancies in the thermomics and select three high-scoring features. The selected features were then added as a multivariate to train a random forest classifier with 100 trees and a maximum depth of two to classify patients into asymptomatic or symptomatic categories [20].

2.4.2. Pretrained CNN

Deep Neural Networks have also found application in conjunction with low-rank matrix approximation, a methodology known as Deep Thermomics [2,19,20,22,23]. In this approach, a pre-trained deep convolutional network, primarily designed for large-scale image recognition, is employed, with ResNet-50 being a notable example [2]. Deep Thermomics relies on low-rank matrix approximation applied to thermal sequences to uncover deep-thermomic features. As ResNet-50 necessitates input in the form of an RGB squared image, this characteristic is ingeniously leveraged to incorporate the initial three bases acquired through sparse-PCT as three input image channels, symbolized as ψ, where $\psi_{\mathrm{RGB}} \rightarrow \psi_{\beta 1\, \beta 2\, \beta 3}$. The utilization of feed-forward convolution in neural network architectures emulates the operation of multiple internal functions within the model, thus enhancing the extraction of intricate features, as:

$$\mathcal{F}(\psi) = \mathcal{F}_L(\ldots \mathcal{F}_2(\mathcal{F}_1(\psi; \{\mathrm{W}_1\}); \{\mathrm{W}_2\}) \ldots; \{\mathrm{W}_\mathrm{L}\}). \qquad \mathcal{F}\colon \mathbb{R}^{224\times224\times3} \tag{9}$$

The residual mapping, $\mathcal{F}_i$, signifies the learning objective within the model, while W_i represents the respective weights assigned to each layer, resulting in the extraction of a total of 2048 features using the pre-trained model [2]. Subsequently, the model underwent an adaptation phase wherein it was transformed into an autoencoder. This adaptation aimed to condense the dimensionality of the initial 2048 features down to a more compact representation consisting of just 16 features. The dimensionality reduction process was executed through the integration of several dense layers of varying sizes situated within the latent space. Notably, this encompassed eight dense layers, with four located in each of the encoder and decoder segments [2]. The network's training regimen involved the utilization of a batch size of 128, spanning a total of 3000 iterations and implementing the Adam optimization algorithm to fine-tune the model. Letting $\mathbf{x} \in \mathbb{R}^F$ where F is 2048, to the latent space $\mathrm{h} = f_e(\mathbf{x}) = a_e(\mathrm{W}\mathbf{x} + \mathrm{b}_\mathrm{e})$ being the hidden representation of the input vector [2]. The main objective for an autoencoder in this case was to minimize $\{\mathrm{W_i}, \mathrm{b_{ei}}\}$ [2] in which it captures the predominant patterns in the data and provides a representation of data that is noise invariant which is extremely important when dealing with how sensitive infrared is to noise.

To enhance the classification of thermal images, a combination of genetic algorithms and convolutional neural networks, including ResNet-50 and DenseNet-201, was employed in the analysis of images sourced from the DMR-IR public database [23]. The dataset comprised images derived from two distinct imaging protocols: static and dynamic. Specifically, this study focused on static images obtained from 176 healthy patients and 39 patients with identified illnesses. In total, 376 images were employed, encompassing 38 patients from each class. Regions of interest (ROIs) were meticulously chosen within breast areas potentially harboring tumors. The images were subsequently subjected to a normalization process utilizing the formula $255 * \frac{(\mathrm{P_{ij}} - \mathrm{L})}{\mathrm{H} - \mathrm{L}}$, where $\mathrm{P_{ij}}$ denoted the pixel value at position (i, j) in the image, H represented the highest pixel value to be normalized, and L signified the lowest value within the dataset [23]. These manually selected regions of interest were further processed, including resizing and the substitution of each pixel's value with a pseudo-color to align with the requirements of convolutional neural networks (CNNs). To facilitate image classification, the CNNs were systematically configured using optimization techniques, with a genetic algorithm being

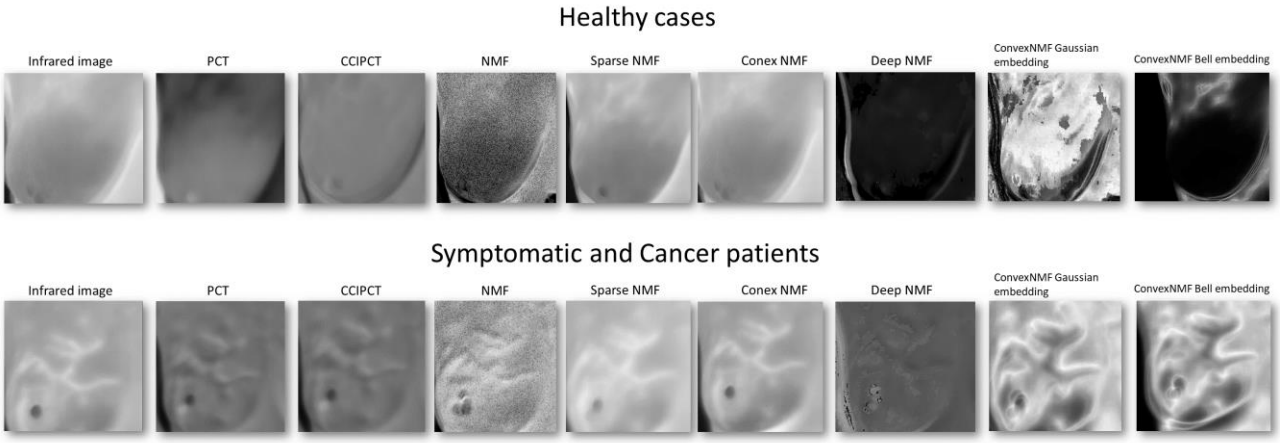

Figure 1. Two examples of healthy and cancer cases for different computational thermography methods.

employed to determine the optimal parameters, encompassing the architecture of the fully connected layers and an optimal learning rate [23].

2.4.3. Sparse Deep-Convolutional Autoencoder Model (SPAER)

To enhance the utilization of the previously mentioned pre-trained models, a novel approach was introduced, referred to as the Sparse Autoencoder (SPAER), aimed at facilitating low-rank approximation of thermal sequences to extract thermomic features for breast cancer diagnosis [22]. The architecture of this proposed autoencoder encompasses both encoding and decoding pathways. These pathways are designed to compress the input data into a lower-dimensional representation and subsequently expand this compressed data to reconstruct the input image with the objective of achieving the closest possible match between the output and the original input [22]. Subsequently, this approach quantifies the loss function and measures the distance between the initial input and the reconstructed output. To optimize the model parameters, a stochastic gradient descent algorithm is applied, ensuring an iterative refinement of the model to achieve the desired output fidelity. The input with the spatial dimension of $512 \times 512 \times 3$, to the latent space dimension of $\boldsymbol{\eta}$, $\boldsymbol{\eta} = F_e(\mathbf{x}) = a_e(\mathrm{W}\mathbf{x} + \mathbf{b}_\mathrm{e})$ is the compressed representation of the input image, a_e is the encoder activation, W and $\mathrm{b_e}$ are the weight and encoder bias matrices, respectively. $\mathrm{y} = \mathrm{G}_d(\boldsymbol{\eta}) = a_\mathrm{d}(\mathrm{W}^\mathrm{T}\boldsymbol{\eta})$ expand the latent features back to the original input spatial dimensions. $\mathbf{y}$ is the equivalent of $\mathbf{x}$ and a_d is the decoder's activation. A deep autoencoder composed of a multilayer model with several activations $a_{(.)_i}$, biases $\mathbf{b}_{(.)_i}$, and weights $\mathrm{W_i}$ matrices with the goal to minimize $\{\mathrm{W}_i, \mathbf{b}_{e_i}\}$ [22]:

$$\mathcal{J}_\mathrm{AE} = \mathbb{E}_\mathbf{x}\left[\ell\left(\mathbf{x}, \mathrm{G}_{\mathrm{d_i}}\left(\mathrm{F}_{\mathrm{e_i}}(\mathbf{x})\right)\right)\right] \tag{10}$$

3. Overview of Models' Accuracies and Discussion

This paper reports an overview of computational thermography using thermomics investigation into the capability of detecting vasodilatation via the identification of heterogeneous thermal patterns, which conducted utilizing datasets obtained from thermal breast cancer screening [26]. Subsequently, the outcomes derived from low-rank approximation via various methodologies developed in this field were juxtaposed against the results obtained through other cutting-edge thermal low-rank matrix approximation algorithms. In addition to these comparisons, a comprehensive assessment of embedding techniques was undertaken across all employed methods. This evaluation served as a crucial step in evaluating the effectiveness of embedding methods as well, which shedding light on the nuances of these diverse approaches.

Hilbert embedded deep low-rank NMF resulted in a cross-validated accuracy of 71.36% (69.42%–73.3%) [19,20], where CCIPCT, PCT, NMF, Sparse PCT, Sparse NMF showed an accuracy range between (62.6%-67.5%) without embedding and improved for (64.6%-72.3%) for a sub-cohort of DMR. This is due to the aggravation of basis through Gaussian embedding. Bell Embedding improved these results by integrating more thermal images up to 77.9%. Bell embedding increases the focus on the heterogeneous thermal patterns in the infrared image. Figure 1 shows the different methods on healthy and cancer cases.

Pretrained CNN model resulted an accuracy, reported by a random forest classifier, 78.16% (73.3-81.07%) between normal and abnormal subjects, which is very close to embedding low-rank methods without going through training of CNN process [24]. These results reported to be challenged using fine-tuning CNN models with an F1-score of 0.92 (DenseNet-201) given to the whole image and 0.90 (ResNet-50) for the breast ROIs [23], while the dataset was divided

(70%-15%-15%) into training, validation, and testing respectively, which highlights the strength of dense CNN. Unfortunately, thermomics in such models due to the end-to-end mechanism is not directly extracted.
SPAER model paired with NMF resulted in accuracies of 78.2% (74.3–82.5%) [22]. These results suggested high performance in SPAER for the preservation of thermal heterogeneity. The model extracts low-dimensional latent space thermomics that can be used for training and testing a model.

4. Conclusion

This study provided an insightful overview of a significant breakthrough in the field of computational thermography, known as thermomics. Thermomics is a methodology geared towards quantifying thermal heterogeneities within dynamic thermography, employing diverse techniques such as low-rank matrix approximation, embedding, and the extraction of features through deep neural networks. The findings of this study comprehensively summarized the application of thermomics within the context of breast cancer screening during the clinical breast examination (CBE) stage. This application underscored the potential for detecting cancer-leading abnormalities (CLAs) that may ultimately progress to breast cancer, demonstrating the practical implications and diagnostic significance of thermomics in this domain.

REFERENCES

[1] R.L. Siegel, K.D. Miller, H.E. Fuchs, A. Jemal, “Cancer statistics” A Cancer J Clin. 2021, 71, 7–33.
[2] B. Yousefi, H. Akbari, X.P.V. Maldague, “Detecting Vasodilation as Potential Diagnostic Biomarker in Breast Cancer Using Deep Learning Driven Thermomics”. Biosensors, 10(11), 164, 2020. Doi: 10.3390/bios10110164
[3] P. Gamagami, “Indirect signs of breast cancer: Angiogenesis study”. Atlas of mammography. Cambridge, Mass: Blackwell Science, 321-6, 1996.
[4] T. Yahara, T. Koga, S. Yoshida, S. Nakagawa, H. Deguchi, K. Shirouzu, “Relationship between microvessel density and thermographic hot areas in breast cancer”. Surgery today, 33(4), 243-248, 2003
[5] N. Rajic (2002). Principal component thermography for flaw contrast enhancement and flaw depth characterisation in composite structures. Composite structures, 58(4), 521-528.
[6] R. Usamentiaga, Y. Mokhtari, C. Ibarra-Castanedo, M. Klein, M. Genest, and X. Maldague, “Automated dynamic inspection using active infrared thermography”. IEEE Transactions on Industrial Informatics, vol. 14, no.12, pp. 5648-5657, 2018.
[7] S. Marinetti, L. Finesso, and E. Marsilio, “Matrix factorization methods: Application to thermal ndt/e,” NDT & E International, vol. 39, no. 8, pp. 611–616, 2006.
[8] K. E. Cramer and W. P. Winfree, “Fixed eigenvector analysis of thermographic NDE data,” in Thermosense: Thermal Infrared Applications XXXIII, M. Safai and J. R. Brown, Eds., vol. 8013, International Society for Optics and Photonics. SPIE, 2011, pp. 225 – 235. [Online]. Available: https://doi.org/10.1117/12.882359
[9] B. Yousefi, H. Memarzadeh Sharifipour, M. Eskandari, C. IbarraCastanedo, D. Laurendeau, R. Watts, M. Klein, and X. P. Maldague, “Incremental low rank noise reduction for robust infrared tracking of body temperature during medical imaging,” Electronics, vol. 8, no. 11, p. 1301, 2019.
[10] J. Ahmed, B. Gao, and W. L. Woo, “Wavelet-integrated alternating sparse dictionary matrix decomposition in thermal imaging cfrp defect detection,” IEEE Transactions on Industrial Informatics, vol. 15, no. 7, pp. 4033–4043, 2018.
[11] M. Barry, M. Khansari, P. D. Tallon, C. Carino, M. Hershman, H.C. Fernandes, O. Haji Maghsoudi, X.P.V. Maldague, B. Yousefi. Multimodal radiothermomic biomarkers for breast cancer screening. In Thermosense: Thermal Infrared Applications XLIV (Vol. 12109, pp. 115-126). SPIE 2022 May, Florida.
[12] B. Yousefi, Sfarra, S., Castanedo, C. I., & Maldague, X. P. (2017). Comparative analysis on thermal non-destructive testing imagery applying Candid Covariance-Free Incremental Principal Component Thermography (CCIPCT). Infrared Physics & Technology, 85, 163-169.
[13] B. Yousefi, S. Sfarra, F. Sarasini, C. I. Castanedo, and X. P. Maldague, “Low-rank sparse principal component thermography (sparse-pct): Comparative assessment on detection of subsurface defects,” Infrared Physics& Technology, vol. 98, pp. 278–284, 2019.
[14] J.-Y. Wu, S. Sfarra, and Y. Yao, “Sparse principal component thermography for subsurface defect detection in composite products,” IEEE Transactions on Industrial Informatics, vol. 14, no. 12, pp. 5594–5600,2018.
[15] C. H. Ding, T. Li, and M. I. Jordan, “Convex and semi-nonnegative matrix factorizations,” IEEE transactions on pattern analysis and machine intelligence, vol. 32, no. 1, pp. 45–55, 2008
[16] B. Yousefi, S. Sfarra, C. Ibarra-Castanedo, N. P. Avdelidis, and X. P. Maldague, “Thermography data fusion and nonnegative matrix factorization for the evaluation of cultural heritage objects and buildings,” Journal of Thermal Analysis and Calorimetry, vol. 136, no. 2, pp. 943–955, 2019.
[17] B. Yousefi, C. Ibarra-Castanedo, and X. P. Maldague, “Infrared nondestructive testing via semi-nonnegative matrix factorization,” in Multidisciplinary Digital Publishing Institute Proceedings, vol. 27, no. 1,2019, p. 13.
[18] B. Yousefi, C.I. Castanedo, & X.P. Maldague (2020). Measuring heterogeneous thermal patterns in infrared-based diagnostic systems using sparse low-rank matrix approximation: Comparative study. IEEE Transactions on Instrumentation and Measurement, 70, 1-9.

[19] B. Yousefi, C.I. Castanedo, & X.P. Maldague, (2020). Low-rank Convex/Sparse Thermal Matrix Approximation for Infrared-based Diagnostic System. arXiv preprint arXiv:2010.06784.
[20] B. Yousefi, H.M. Sharifipour, & X.P. Maldague (2021). A Diagnostic Biomarker for Breast Cancer Screening via Hilbert Embedded Deep Low-Rank Matrix Approximation. IEEE Transactions on Instrumentation and Measurement, vol. 70, pp. 1-9, 2021, Art no. 4504809, doi: 10.1109/TIM.2021.3085956.
[21] Yousefi, B., Hershman, M., Fernandes, H. C., & Maldague, X. P. (2021). Concentrated Thermomics for Early Diagnosis of Breast Cancer. Engineering Proceedings, 8(1), 30.
[22] Yousefi, B.; Akbari, H.; Hershman, M.; Kawakita, S.; Fernandes, H.C.; Ibarra-Castanedo, C.; Ahadian, S.; Maldague, X.P.V. SPAER: Sparse Deep Convolutional Autoencoder Model to Extract Low Dimensional Imaging Biomarkers for Early Detection of Breast Cancer Using Dynamic Thermography. *Appl. Sci.* **2021**, *11*, 3248.
[23] Gonçalves, C. B., Prado Domingos, A. C., Yousefi, B., Souza, J. R., & Fernandes, H. (2022). Effects of Region of Interest on Breast Cancer Detection using CNN and Infrared Imaging
[24] N. Vigil, B. M. Nouri, H. C. Fernandes, C. Ibarra-Castanedo, X. P. V. Maldague and B. Yousefi, "Convex Factorization Embedding Thermography for Breast Cancer Diagnostic," in *IEEE Open Journal of Instrumentation and Measurement*, vol. 1, pp. 1-8, 2022, Art no. 4500408, doi: 10.1109/OJIM.2022.3203452.
[25] Leonardo D. Buitrago, Jimmy J. Azarnoosh, Xavier P. V. Maldague, and Bardia Yousefi "Optimal thermomic biomarkers for early diagnosis of breast cancer", Proc. SPIE 12536, Thermosense: Thermal Infrared Applications XLV, 1253611 (12 June 2023); https://doi.org/10.1117/12.2663835
[26] L. Silva, D. Saade, G. Sequeiros, A. Silva, A. Paiva, R. Bravo, and A. Conci, “A new database for breast research with infrared image,” Journal of Medical Imaging and Health Informatics, vol. 4, no. 1, pp.92–100, 2014.